

Grid-Forming Inverter-based Wind Turbine Generators: Comprehensive Review, Comparative Analysis, and Recommendations

Thai-Thanh Nguyen, *Member, IEEE*, Tuyen Vu, *Member, IEEE*, Sumit Paudyal, *Member, IEEE*, Frede Blaabjerg, *Fellow, IEEE*

Abstract—High penetration of wind power with conventional grid following controls for inverter-based wind turbine generators (WTGs) reduces grid inertia and weakens the power grid, challenging the power system stability. Grid-forming (GFM) controls are emerging technologies that can address such stability issues. Numerous methodologies of GFM inverters have been presented in literature; however, their applications for WTGs have not been thoroughly explored. As WTGs need to incorporate multiple control functions to operate reliably in different operational regions, the GFM control should be appropriately developed for the WTGs. This paper presents a review of GFM controls for WTGs, which covers the latest developments in GFM controls, including multi-loop and single-loop GFM, virtual synchronous machine-based GFM, and virtual inertia control-based GFM. A comparison study for these GFM-based WTGs is then illustrated. In addition, the challenges of applying these GFM controls to wind turbines are discussed, including the impact of DC-link voltage and the current saturation algorithm on the GFM control performance. Finally, recommendations and future developments of GFM-based wind turbines to increase the power system reliability are presented.

Index Terms—Wind turbine generator, grid-forming inverter, virtual synchronous generator, wind farm, inertia support.

I. INTRODUCTION

WIND turbine generators, especially for offshore wind farms, are growing in both size and power rating to reduce the Levelized cost of energy. GE has launched the 12-14 MW Haliade-X offshore turbine in 2021 [1], while Vestas has also introduced 10 MW offshore turbines since 2018 and 15 MW offshore wind turbine since 2021 [2], [3], to name a few. In 2020, National Renewable Energy Laboratory (NREL) released the International Energy Agency (IEA) 15 MW offshore reference wind turbine [4]. Multi-megawatt wind turbines are typically coupled with the power conversion systems to increase the efficiency of wind turbines and support grids under normal and abnormal operations. Controls of power conversion systems in multi-megawatt wind turbines for large wind farms will play an essential role in improving the power system stability with high wind penetration.

Typical turbine controllers are based on the grid-following (GFL) techniques, in which the phase-locked loop (PLL) is used to track the instantaneous angle of the point of common coupling (PCC) voltage, and the current control loop is used to regulate the AC current reflecting active and reactive power

This work is supported by the New York State Energy Research and Development Authority (NYSERDA) - award number 148516. T. T. Nguyen and T. Vu are with Clarkson University, NY, USA; S. Paudyal is with Florida International University, FL, USA. F. Blaabjerg is with Aalborg University, Denmark. Emails: tnguyen@clarkson.edu, tvu@clarkson.edu, spaudyal@fiu.edu, fbl@energy.aau.dk. Corresponding Author: T. Vu, Email: tvu@clarkson.edu

injected into the grid. The main issue in using PLL is that it negatively reduces the power converter stability's margin, especially when the grid condition is weak [5]. The instability of multi-megawatt wind turbines will result in more severe impacts on the overall power system stability. Grid-forming (GFM) controls can address the instability issues of wind turbines under weak grid conditions as they do not require the PLL [6]. A wind turbine with GFM control behaves as a controllable voltage source behind a low-output impedance, which forms the voltage amplitude and frequency of the local grid. Thus, the GFM wind turbines can operate independently from the main power grid and possesses the black start capability with a sufficient energy buffer. Successful trial of a recent 69 MW wind park operated in the GFM mode reveals GFM wind turbines' potentials with additional promising inertia support and black start capability [7], [8].

While the definition of the GFM controls is being considered in industrial and academic communities, various GFM structures for wind turbines have been introduced [9]–[12]. Although there are exiting review studies of GFM inverters [13]–[16], they do not cover applications for wind turbines. Since the control systems of wind turbines are complex with multiple operational regions, along with multiple control functions, such as maximum power point control, constant torque/speed control, voltage-ride through control, etc., the uses of GFM controls in wind turbines should be carefully considered to ensure that all functions are preserved. Therefore, realizing GFM controls for wind turbines is a crucial asset for the development of power systems with high penetrations of wind. In this context, this paper aims to contribute the following.

- This paper comprehensively reviews state-of-the-art GFM controls of wind turbines. Challenges and issues in deploying GFM controls for wind turbines are discussed.
- A comparative study of different types of GFM controls for wind turbines is carried out to reveal their advantages and disadvantages.
- Future directions and recommendations for wind turbines are provided that suits grid functionalities sought.

The rest of this paper is organized as follows. Section II briefly summarizes the typical control blocks of the GFL wind turbine generator as the majority of controllers in the GFM WTG is the same as the GFL WTG. Section III reviews the state-of-the-art GFM controls of wind turbine generators and presents four types of GFM controls used in this paper for the comparative study. The comparative analysis of these GFM controls under normal and abnormal conditions is presented in Section IV. Future direction and recommendations are

provided in Section V. Finally, Section VI summarizes the main findings of this paper.

II. GRID-FOLLOWING WIND TURBINE GENERATORS

Utility-scale wind turbines are typically based on two types of generators: Type 3 with the doubly fed induction generator (DFIG) and Type 4 with the permanent magnet synchronous generator (PMSG). The former equips with a partial-scale power converter, while the latter equips with a full-scale power converter. Although Type 4 WTG can use other types of generators, such as squirrel cage induction generator (SCIG), wound rotor synchronous generator (WRSG), and high-temperature superconducting synchronous generator (HTS-SG), PMSG-based Type 4 is preferred due to its advantages of high efficiency, high power density and reliability [17]. PMSG-based WTG offers a variety of advantages compared to the DFIG type. For instance, using a full-scale power converter allows the generator to fully decouple from the grid and provide a wider range of controllability. The gearbox system is used in the PMSG-based WTG to reduce the size and weight of generators. However, due to high maintenance cost and the risk of gearbox failure, the direct-driver PMSG that eliminates the gearbox system from the wind turbines are growing in popularity. As the PMSG-based WTG is becoming the preferred technology [18], this paper mainly focuses on the grid-forming control of this type for the review and analysis.

As the majority of controllers in the GFM WTG is the same as the conventional GFL WTG, this section briefly summarizes the GFL control of Type-4 WTG. An overall configuration of Type-4 WTG is shown in Fig. 1, which consists of a wind turbine, a permanent magnet synchronous generator (PMSG), a back-to-back (BTB) converter including machine-side converter (MSC), and a grid-side converter (GSC), a DC chopper, grid filters, and a step-up transformer. The main control system includes a pitch controller, a machine-side controller, and a grid-side controller.

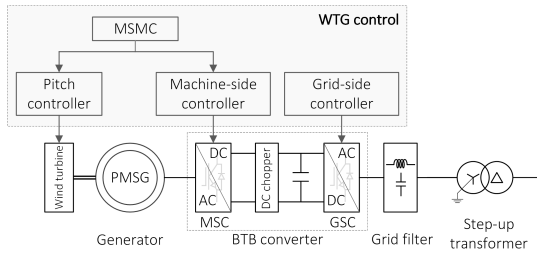


Fig. 1. Configuration of Type-4 wind turbine generator and its control system.

(MSMC). The pitch controller regulates the blade pitch angle in conditions of a high wind speed or curtailing wind power. The grid-side controller is responsible for maintaining the DC-link voltage of the BTB converter, whereas the machine-side controller is in charge of regulating generator torque. The MSMC generates the reference signals for the machine-side and pitch controllers, performing various operation modes of WTG, such as normal mode with different operating regions and power curtailment mode.

The detailed schematic diagram of the GFL WTG is shown in Fig. 2 (extension of Fig. 1). Both grid-side and machine-side controllers include multi-loop control structure, including an inner current loop and outer DC-link voltage control or torque control loop. The grid-side controller is designed with the grid-following control scheme, in which PLL is used to track the instantaneous angle of the terminal voltage. The proportional-integral (PI) regulators are used to control voltage and current in dq frame. The rotor speed (ω_r) is used for the machine-side controller to generate the instantaneous phase angle (θ_r). The detailed schematic diagram of grid-side and machine-side converters can be found in [19].

The reference signals for the pitch and machine-side controllers depend on the wind speed condition and the reference power from wind plant-level control. An additional outer control loop generates these reference signals, which is represented by the block diagram in existing studies [20]–[22]. However, in this paper MSMC, which has the same functionality as such outer loop, is introduced for the sake of simplicity, as given by **Pseudocode 1**. In power curtailment mode, the pitch controller regulates rotor speed at the rated value ($\bar{\omega}_r$) while the machine-side controller regulates the output wind power. Otherwise, the wind turbine generator operates under four main regions depending on the wind speed condition, as shown in Fig 3. The wind turbine is turned off in regions 1 and 4 where the wind speed is lower than the cut-in speed (v_{c-in}) or higher than the cut-out speed (v_{c-out}), respectively. To avoid 3-period interference effects, the pitch controller regulates rotor speed at minimal value (ω_{min}) in Region 1.5 [4] where the wind speed is higher than the cut-in speed but lower than the wind speed caused interference (v_{inter}). In Region 2, where the wind speed is higher than the v_{inter} but lower than the rated wind speed (\bar{v}_w), the pitch controller is disabled, and the generator torque is regulated optimally to maximize the wind power, in which the optimal gain (k_{opt}) is given by (1).

$$k_{opt} = 0.5\rho\pi R^2 C_p^{\max} (R/\lambda_{opt})^3. \quad (1)$$

where ρ is the air density; R is the turbine rotor radius; C_p^{\max} is the maximal rotor power coefficient; and λ_{opt} is the optimal

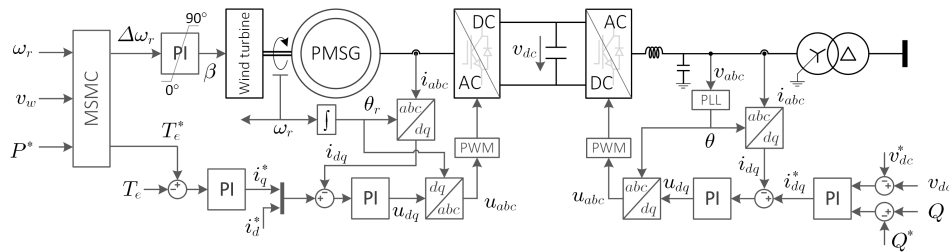


Fig. 2. Typical grid-following control of wind turbine generator.

Pseudocode 1 Machine-side master control.

```

1: if  $P^* < \bar{P}$  then % Power curtailment
2:    $\Delta\omega = \omega_r - \bar{\omega}_r$ 
3:    $T_e^* = P^*/\omega_r$ 
4: else
5:   if  $v_w < v_{c\text{-in}}$  then % Region 1
6:      $\Delta\omega = 0$ 
7:      $T_e^* = 0$ 
8:   else if  $v_{c\text{-in}} \leq v_w < v_{\text{inter}}$  then % Region 1.5
9:      $\Delta\omega = \omega - \omega_{\min}$ 
10:     $T_e^* = k_{\text{opt}}\omega_r^2$ 
11:   else if  $v_{\text{inter}} \leq v_w < \bar{v}_w$  then % Region 2
12:      $\Delta\omega = 0$  % Force  $\beta = 0$ 
13:      $T_e^* = k_{\text{opt}}\omega_r^2$ 
14:   else if  $\bar{v}_w \leq v_w < v_{c\text{-out}}$  then % Region 3
15:      $\Delta\omega = \omega_r - \bar{\omega}_r$ 
16:      $T_e^* = \bar{T}_e$ 
17:   else % Region 4
18:      $\Delta\omega = 0$ 
19:      $T_e^* = 0$ 
20:   end if
21: end if

```

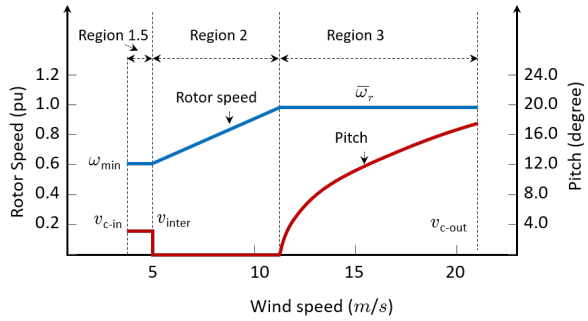


Fig. 3. Operating regions of WTG. Note that regions 1 and 4 are not shown in the figure.

tip-speed ratio. When the wind speed is higher than the rated wind speed but lower than the cut-out speed, the wind turbine operates on Region 3. In this region, the pitch controller is activated to regulate the rotor speed and generator torque at the rated values ($\bar{\omega}_r$ and \bar{T}_e).

III. GRID-FORMING CONTROL OF WTG

Unlike the GFL WTG, the DC-link voltage of the GFM WTG can be regulated by either grid-side, machine-side, or external converters. Existing studies categorized grid-forming inverters based on the GFM control methodologies, which is appropriate as the DC-link voltage is assumed to be constant. However, for wind turbine applications, the strategy of DC-link voltage regulation must be considered because it affects the implementation of WTG's control system. This paper categorizes the GFM WTGs based on the regulation strategies of DC-link voltage, as shown in Fig. 4. The GFM WTGs are classified into three categories:

- G-GFM: GSC controls the DC-link voltage.
- M-GFM: MSC controls the DC-link voltage.
- E-GFM: External energy storage system controls the DC-link voltage.

In each category, two types of GFM controls are classified according to the inner control loop of the grid-forming controller: the multi-loop control (MGFM) and single-loop control (SGFM). The MGFM types include the inner current and AC voltage control loops, while the SGFM types consist of only the AC voltage control loop.

The first category of GFM-WTG is the G-GFM, in which the grid-side converter controls the DC-link voltage. An outer DC-link regulator is designed in addition to the inner control loop of the grid-side converter. The DC-link voltage is controlled by adjusting the instantaneous phase angle of the terminal voltage. The DC-link voltage regulators mimic the inertia support of the synchronous generator by allowing the variation of DC-link voltage in an acceptable range, which has been presented in different names, such as virtual inertia control (VIC) [23], [24], inertia synchronous control (ISynC) [25], and power synchronous control [10]. The main advantage of this type is the least effort in developing the GFM WTG from the typical GFL WTG as only the grid-side controller is different. The pitch and machine-side controllers are kept the same as the GFL type.

The second category of GFM WTG is the M-GFM, in which the machine-side converter regulates the DC-link voltage, whereas the grid-side converter is designed for managing output power. The grid-forming controllers implemented in the grid-side converter also mimic the inertia characteristic of synchronous generators, although different controller names have been presented, such as VIC [26], virtual synchronous machine (VSM) [9], [12], [27]–[29], and synchronverter [30].

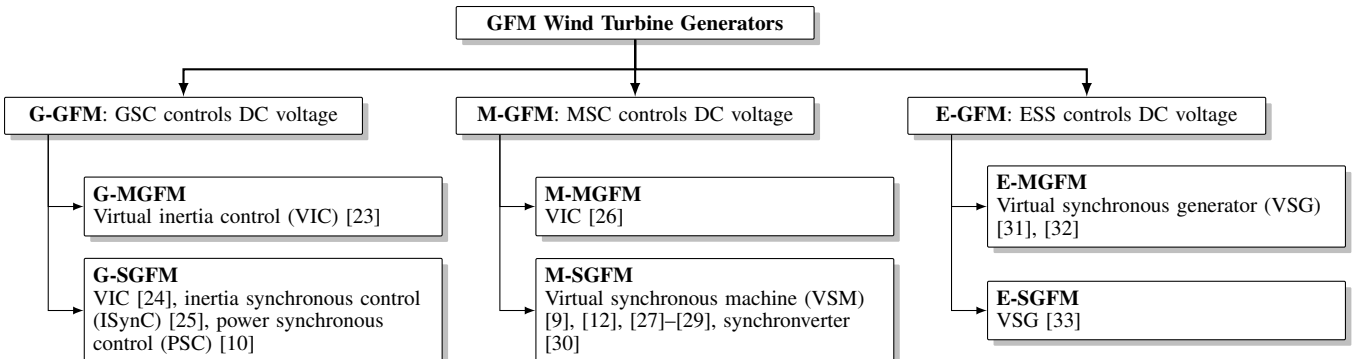


Fig. 4. Existing grid-forming controls of wind turbine generators.

This method requires much effort in developing the GFM control system from GFL WTG as both grid-side, and machine-side controllers must be modified.

The last category of GFM WTG is the E-GFM, in which the DC-link voltage is controlled by an external energy storage system (ESS). This approach provides an additional degree of freedom for grid-side controllers while retaining all control functions of pitch and machine-side controllers. VSG-based GFM controls are mainly used in this type [31]–[33]. As the DC-link voltage is managed constantly by the external ESS, most exiting GFM methodologies available in literature can be used for the grid-side converter without any modification, such as droop control, power synchronization control, and virtual synchronous generator [5], [34], [35]. It is anticipated that using additional ESS devices introduces technical benefits because ESS can play the role of energy buffer to mitigate the fluctuations in wind power or support grid during the disturbance. However, this GFM type increases the complexity of the WTG control system and total investment cost.

Overall, it can be found that all existing GFM control methodologies for WTGs try to mimic the inertia characteristic of synchronous generator. This paper investigates only G-GFM and M-GFM categories as they are potential solutions for developing GFM WTG from the existing GFL type. Among two categories, four types of GFM WTGs will be presented in the following sections, which are:

- G-GFM with multi-loop control (G-MGFM)
- G-GFM with single-loop control (G-SGFM)
- M-GFM with multi-loop control (M-MGFM)
- M-GFM with single-loop control (M-SGFM)

To ensure a fair comparison, the G-MGFM and G-SGFM types use the same outer VIC scheme, while M-MGFM and M-SGFM types use the same outer VSM scheme. The blue color depicts the difference between the GFM and GFL controls of WTGs in the schematic diagram in the following sections. The DC chopper and reactive power control loop of GSC are omitted in the explanation as they are the same for all GFM and GFL control methods.

A. **G-GFM:** Grid-side converter controls DC link voltage

Like the GFL control of WTG, the GSC in the G-GFM category is responsible for regulating DC-link voltage. How-

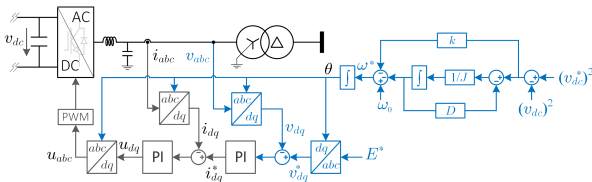


Fig. 5. Schematic diagram of G-MGFM wind turbine generator.

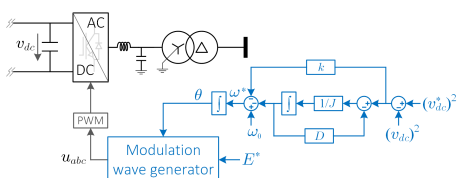


Fig. 6. Schematic diagram of G-SGFM wind turbine generator.

ever, the grid-forming control scheme is used for the grid-side controller. The VIC scheme controls the DC-link voltage, which generates the instantaneous phase angle reference for the inner control loop. According to the structure of inner control loop, this control approach is classified into multi-loop control type (G-MGFM) [23] and single-loop control type (G-SGFM) [10], [24], [25].

The schematic diagram of the G-MGFM control of WTG is shown in Fig. 5, where the difference between G-MGFM and GFL controls is shown in the blue color. The machine-side controller of the G-MGFM WTG is the same as the GFL WTG, which is omitted in this figure. The grid-side controller utilizes a cascaded control structure that includes an inner current control loop and outer AC voltage control loop, which plays a role in forming the terminal voltage [36]. The instantaneous phase angle is directly generated from the reference angular frequency rather than the use of PLL. The angular frequency reference is adjusted to regulate the DC-link voltage of the BTB converter by the virtual synchronous control loop in [10], as given by (2). The virtual inertia control utilizes the DC-link as an energy buffer to mimic the behavior of synchronous machine.

$$\omega^* = \omega_0 - \left(k + \frac{1}{J_S + D} \right) (v_{dc}^{*2} - v_{dc}^2), \quad (2)$$

where $\omega_0 = 2\pi f$; k is the tracking coefficient; J is the inertia coefficient; and D is the damping coefficient.

The schematic control diagram of the G-SGFM is shown in Fig. 6, in which the modulation signal (u_{abc}) is generated directly from the instantaneous phase angle (θ) and reference of voltage amplitude (E^*). The modulation wave generator is given by (3).

$$u_{abc} = E^* \begin{bmatrix} \sin(\theta) & \sin(\theta - \frac{2\pi}{3}) & \sin(\theta + \frac{2\pi}{3}) \end{bmatrix}^\top. \quad (3)$$

As the role of the grid-side controller is the same as GFL WTG, the pitch and machine-side controllers, including MSMC, are the same as GFL WTG. Thus, all control functions such as region controls and power curtailment are retained without any modification.

B. M-GFM: Machine-side converter controls DC link voltage

The schematic diagrams of the M-MGFM and M-SGFM types are shown in Figs. 7 and 8, respectively. Unlike the GFL WTG, the DC-link voltage of the BTB converter is controlled by the machine-side converter, while the grid-side controller is in charge of regulating the output power of the wind turbine generator. As the control strategies of grid-side and machine-side converters are switched, control in region 2 is modified to retain the control functions of GFL WTG. Instead of optimal torque control to maximize wind power in region 2, the M-GFM manages optimal power (P^*) that is calculated by multiplying optimal torque by rotor speed, as given by (4). The MSMC is the same as GFL WTG.

$$P^* = T_e^* \omega_r. \quad (4)$$

The virtual synchronous machine (VSM) scheme in [9] is used for the outer control loop in this M-GFM category. The reference of angular frequency is adjusted to manage the output power of WTG, as given by (5).

$$\omega^* = \omega_0 - \frac{1}{J\varsigma + D} (P^* - P), \quad (5)$$

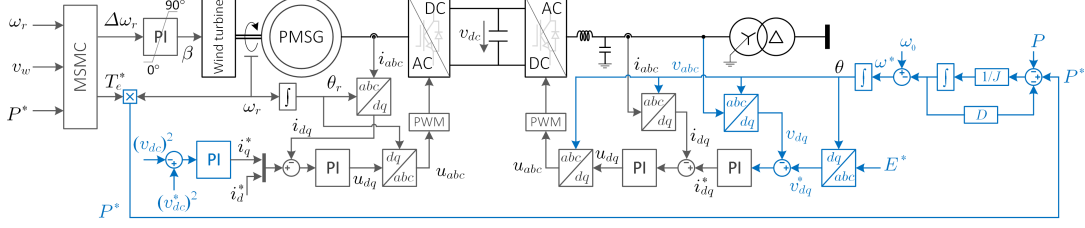


Fig. 7. Schematic diagram of M-MGFM wind turbine generator.

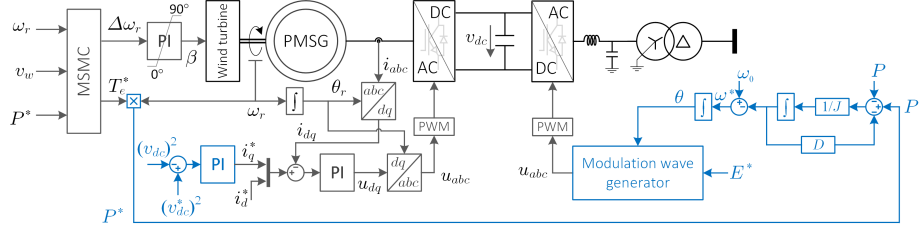


Fig. 8. Schematic diagram of M-SGFM wind turbine generator.

where P is the measured output power of wind turbine generator.

The cascaded control structure with inner current and voltage control loops is used in the M-MGFM type [26] whereas only voltage control loop is used in the M-SGFM type [9], [12], [27]–[30]. The schematic diagram of the M-SGFM wind turbine generator is shown in Fig. 8, which is the same as M-MGFM control, except the inner controller of the grid-side converter. To generate modulation signals (u_{abc}), the modulation wave generator from (3) is used in the M-SGFM type.

IV. COMPARATIVE ANALYSIS

This section discusses comparative results for five control strategies of WTG: GFL control and four types of GFM controls. A 15 MW direct-drive Type-4 WTG is used to evaluate the control performance of these control strategies. The parameter of 15 MW WTG is given in [20]. Firstly, the operation of WTG under the condition of dynamic-wind speed is conducted to evaluate the performance of the region control function. Secondly, under high wind speed conditions, the power set-point of WTG is changed to test the function of power curtailment. Finally, the three-phase-to-ground fault is used to evaluate the responses of these control strategies under abnormal conditions. For all the above scenarios, the grid's strength is also taken into consideration. It should be noted that the parameters of VIC and VSM of all GFM types are the same to ensure a fair comparison in this paper. However, these parameters can be properly designed to obtain the desired performance.

A. Normal Operation

This section evaluates the performance of the region control function. The wind speed changes from 7 m/s to 15 m/s at 30 s, resulting in WTG operation in regions 2 and 3. The compared result of GFL and GFM controls under strong grid conditions is shown in Fig. 9, in which the short-circuit ratio (SCR) is

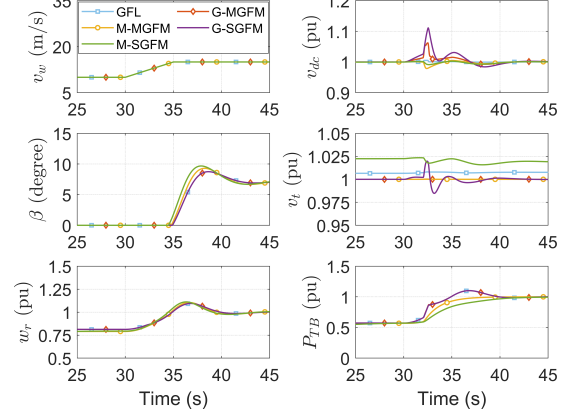


Fig. 9. Performance of region control mode under strong grid (SCR = 10).

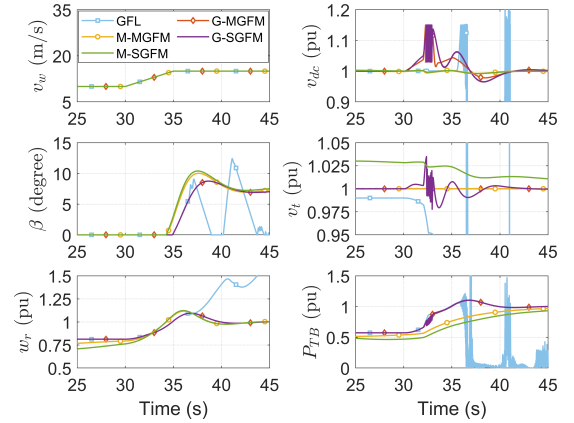


Fig. 10. Performance of region control mode under weak grid (SCR = 2.5).

equal to 10. It can be seen the difference in transient behaviors from this figure. The G-GFM (G-SGFM and G-MGFM) and GFL types show the same transient responses in active power, rotor speed, and pitch angle, as they have the same machine-

side controllers. The difference between these controllers is observed in DC-link voltage and terminal AC voltage. The G-GFM types cause significant transient in DC-link voltage compared to the GFL type. The terminal AC voltage is kept constant with the G-MGFM type like the GFL control, whereas the transient AC voltage is observed in the G-SGFM type. The M-GFM (M-MGFM and M-SGFM) types stably regulate the DC-link and terminal AC voltage without any significant transient as the machine-side converter controls the DC-link voltage. It also can be observed that there is no overshoot of active power response under M-GFM controls, compared to GFL and G-GFM controls.

The comparison of these controllers in weak grid conditions is shown in Fig. 10, in which the SCR value is 2.5. It can be seen that the GFL control fails to keep the WTG in stable operation, whereas all types of GFM controls stably operate. However, the performance of these GFM controls under weak grid conditions is also different. Compared to the strong grid condition, the G-GFM types preserve their performance in regulating rotor speed and output power; however, the performance of DC-link voltage regulation is slightly degraded. It can be seen that the DC chopper is activated to protect the DC system in the case of G-GFM controls. Although the M-GFM types stably regulate the DC link and terminal AC voltage, slow response time in rotor speed and output power is a drawback of these controls under weak grid conditions, as depicted in waveform rotor speed and output power from 25 s to 30 s.

The power set-point of WTG is changed from 1 pu to 0.8 pu to evaluate the performance of power curtailment mode. In this mode, the pitch controller regulates the rotor speed of PMSG constantly at 1 pu. The G-GFM types regulate the output power of WTG through the torque controller, whereas the M-GFM types directly regulate output power. Fig. 11 shows the comparison of five controllers in strong grid conditions. It can be seen in G-GFM types that the sudden change in the torque reference causes a rapid drop of DC-link and terminal AC voltage. The advantage of these GFM types is the fast response of output power; however, significant transient in DC-link and terminal AC voltage is observed. In the cases of M-GFM types, the output power of the wind turbine is directly regulated via the VSM scheme of the grid-side controller. Although the output power response with these M-GFM types is slow, the DC-link voltage and terminal AC voltage are stably maintained. The comparison in the condition of the weak grid is shown in Fig. 12. The GFL type fails to control WTG in this condition. In comparison to the strong grid state, the G-GFM types exhibit more substantial transients in DC-link voltage and terminal AC voltage, whereas the M-GFM types show slower response in output power.

B. Abnormal Operation

The advantage of the MGFM types is limiting fault currents by the inner current control loop. By comparison, limiting fault currents in the SGFM types is challenging due to the lack of the inner current control loop. Various studies have proposed the overload mitigation control scheme to limit the fault current. In this paper, the GFL, G-MGFM, and M-MGFM types use the current saturation scheme in [37] with a maximum current of 1.2 pu, and the G-SGFM and M-

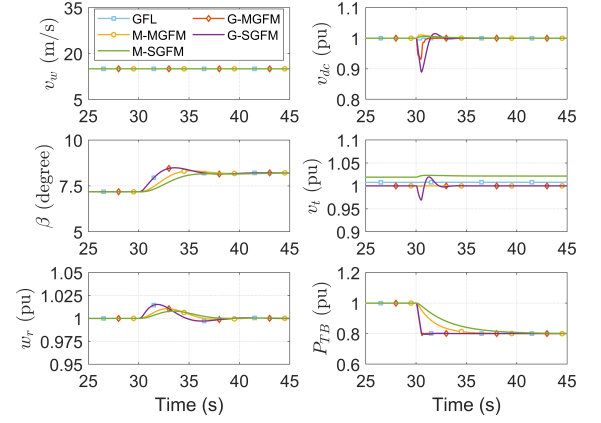


Fig. 11. Performance of power curtail mode under strong grid (SCR = 10).

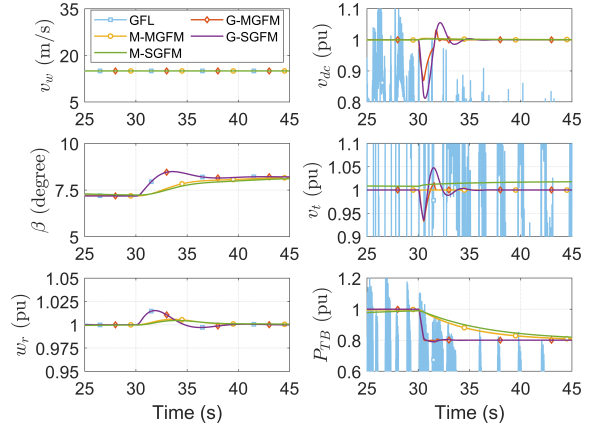


Fig. 12. Performance of power curtail mode under weak grid (SCR = 2.5).

SGFM types use the overload mitigation scheme in [38] with a maximum power of 1.2 pu.

Performance of GFL and GFM controls of WTG under three-phase-to-ground fault is shown in Figs. 13 and 14. It can be seen that the response of each control strategy under a fault condition is different. For the typical GFL control, the DC-link voltage rapidly increases when the fault occurs because the GFL control slowly responds to the disturbance. When the DC-link voltage increases significantly, the DC-chopper is activated to protect the DC system. However, the response of GFM controls is different. Because the GFM WTGs respond quickly to the disturbance while the electric power from PMSG changes slowly, DC power from the DC link is drawn to compensate for the disturbance, resulting in the rapid drop of DC-link voltage. This phenomenon causes a negative impact on the control performance of GFM WTG. In addition, the current saturation in multi-loop GFM types causes the phase shift, making MGFM types difficult to recover after clearing the fault. It can be seen that the GFM controls under strong grid conditions tend to lose synchronism easier than the weak grid condition as a small change in phase angle causes significant power oscillation. The M-GFM types gain the advantage in this condition as the machine-side converter controls the DC-link voltage. The DC-link voltage can easily be recovered after clearing the fault, making WTG stably restore to steady-state condition.

Fig. 15 shows the three-phase current of GFL and GFM

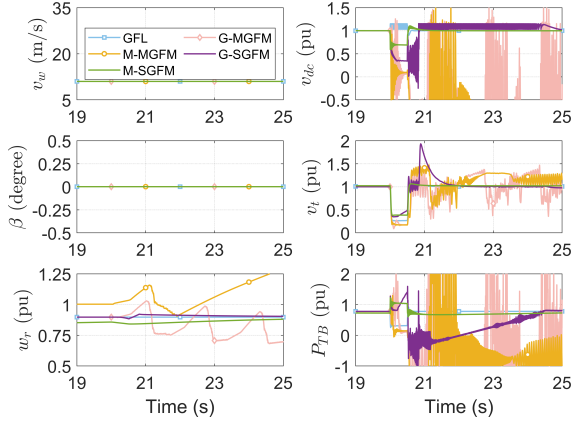


Fig. 13. Fault performance under strong grid. The G-MGFM and M-MGFM types tend to instability.

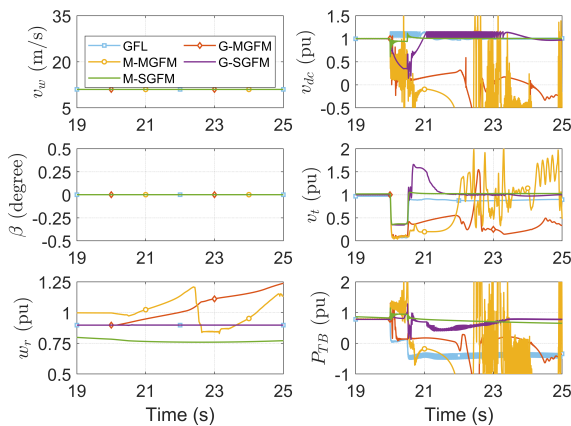


Fig. 14. Fault performance under weak grid. The GFL, G-MGFM, and M-MGFM types tend to instability.

controls. It can be seen that the GFL control successfully limits the transient current at 1.2 pu when the grid is strong. All GFM controls fail to limit the transient current. It should be noted that the current saturation scheme of GFL and multi-loop GFM types are the same. It is also observed that the transient current of GFM controls in strong grid conditions is much higher than the weak grid condition. After clearing the fault, the multi-loop GFM types lose synchronization due to the current saturation. By comparison, the SGFM types still synchronize with the grid during fault by the overload control scheme, which helps WTG restore to the normal operation.

V. RECOMMENDATIONS AND FUTURE DIRECTION

A. Recommendations

1) *Stability of GFM WTG:* The detailed comparisons between multi-loop and single-loop GFM inverters in microgrids [39] revealed that the stability margin of the single-loop control is larger than the multi-loop control; however, the stability issues of GFM WTGs have not been evaluated. Our paper performed fault studies to evaluate the stability margin of different GFM control methodologies for WTGs. It is also revealed that the single-loop GFM WTG provides a larger stability margin than the multi-loop control of WTG. Figs. 13 and 14 depicted that the MGFM types tend to instability while the SGFM types are stable. The stability margin of the

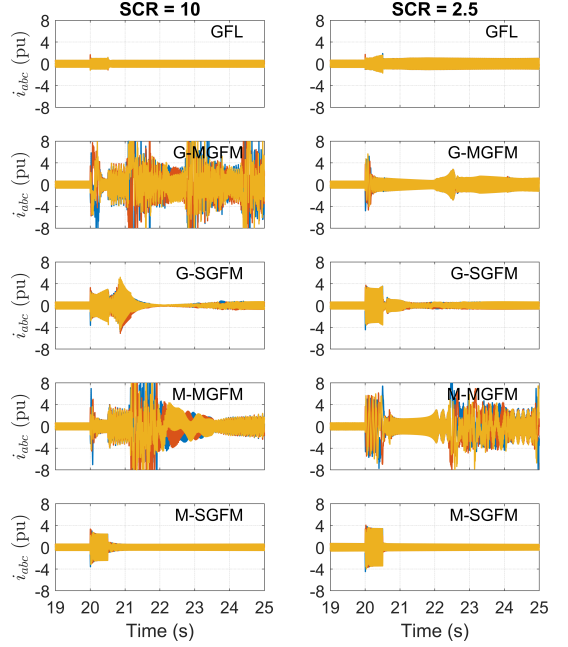


Fig. 15. Three-phase transient current of WTG under fault condition.

GFM WTG depends on the GFM control structure and the regulation strategies of DC-link voltage. Specifically, M-GFM types can stably restore to the normal operation after clearing the fault, whereas the G-GFM types experience severe disturbance or even instability. The M-GFM types provide a better performance as the machine-side converter controls the DC-link voltage which is decoupled from the grid's disturbance. However, the active power response of M-GFM types under normal operation relies on the grid's strength. Thus, an optimal design of virtual synchronous machine for the M-GFM types should be considered.

2) *Current limiting strategy:* Due to the lack of the current control loop, the SGFM types face the challenge of limiting the transient current. As depicted in Fig. 15, although the SGFM types stably recover in the post-fault condition with overload mitigation control scheme, transient current of SGFM types during fault reaches 5 pu, which can damage the power converter. Since existing current saturation scheme of GFL control cannot be used for the MGFM types, different current limiting strategies have been developed, such as switching control strategy from grid-forming to grid-following during fault period [40], virtual active power [41], using virtual impedance or admittance in addition to current saturation algorithm [42]–[44], current reference limiting with anti-windup integration [45], current-constrained unified virtual oscillator control [46], and circular current limiter [47]. Most existing current limiting strategies have been developed for the multi-loop GFM controls. As the single-loop GFM controls provide a better performance, further research should be conducted on the current limiter for these GFM controls. In addition, existing current limiting strategies have been developed without considering the dynamic behavior of DC-link voltage during the disturbance, which might be inappropriate for wind turbine applications as the DC-link voltage of WTG varies significantly during fault conditions. A detailed analysis of these current limiting strategies on the full WTG model is

essential to verify their feasibility to wind turbine applications.

3) *Fault Ride-Through Capability*: Various open issues of GFM inverters, such as grid synchronization, current limiting, and fault ride-through, have been discussed in [5], [35], which persist for the wind turbine applications. Critical clearing time is an essential factor of GFM controls to maintain grid synchronization in post-fault condition [34], [40], [42], [48]. The fault ride-through strategy should be developed in conjunction with current limiting [43], [46]. Developing the voltage ride-through strategy in accordance with the international standards is crucial for practical studies of GFM WTGs.

4) *Sub-synchronous and harmonic resonance*: Subsynchronous control interaction (SSCI) of Type-4 WTG, which is caused by interaction between controllers of WTGs and series compensated line, have been reported in [49], [50]. Harmonic resonance is caused by interaction among WTG's controllers and shunt capacitance of offshore transmission cable or shunt capacitors, which has been reported in Toronto system [51]. The resonance frequency of SSCI is typically between 1 and 10 Hz, whereas the frequency of harmonic resonance is in second or third order frequency. These resonance issues have been observed in the GFL control of WTG. A recent study in [52] demonstrated that the single-loop GFM control also experienced the SSCI issue. More detailed analysis on SSCI and harmonic resonance of GFM WTG should be conducted.

5) *Wind turbine structural loads*: Electro-mechanical interactions, in which the grid disturbances cause the structural vibration of wind turbines, have been investigated for the GFL wind turbines [53], [54]. The grid-code requirements pose challenges for the design of the mechanical structure and the electrical system of wind turbines [55], [56]. The control systems of wind turbines can be appropriately designed to mitigate such interactions [57], [58]. The issue of electro-mechanical interactions is even worse in the case of GFM WTG, especially offshore floating GFM wind turbines. Phase jumps are the most stressful events for the GFM WTG, which results in the rapid increase of current in the GFM WTG and large torque/power oscillations [59]. Such oscillations have a severe impact on the wind turbine structural loads. It is required to investigate the impacts of the GFM control methodologies on the wind turbine structural loads.

6) *Protection of GFM WTG-based wind farms*: The fault current contribution from the inverter-based resources is limited due to the hardware constraints, which poses a challenge to the protection systems. The lack of negative sequence current injection is another challenge as the protection systems rely on negative sequence components to detect the unbalanced fault [60]. The German grid codes require the ability to inject negative sequence component [61]. Although existing multi-loop GFM controls lack the ability to inject the negative sequence component, the sequence-based control strategy can be used to control the negative sequence component [62], [63]. By comparison, the single-loop GFM types can supply both negative and zero sequence components, which is experimental verified in [64].

B. Future Direction

1) *Technical standards*: Existing IEEE 1547 standard [65] was developed for the GFL inverters, which emphasize reactive power limits, current harmonic limits, and anti-islanding

features [13]. However, these requirements need to be revisited to apply for the GFM inverters which have distinct behaviors from the GFL inverters. For example, as the GFM inverters have the ability to operate in the stand-alone mode due to their voltage-source behavior, the requirement of the anti-islanding function is obsolete. The National Electric Reliability Corporation (NERC) standard PRC-024-2 is used for protective relay settings, which ensures the voltage and frequency ride-through capabilities of generating units [66]. However, the frequency limits in this standard, which was based on the limitations of synchronous machines, might not be a suitable metric for tripping inverter-based resources. NERC issued the performance guideline for inverter-based resources [67], which indicated that the voltage and frequency trip settings should be set as wide as possible. On the other hand, a Grid-code technical specification for GFM inverters has been proposed by National Grid ESO in [68], which emphasizes inertia active power, fast fault current injection, and phase jump. These issues have also been discussed by the European Network of Transmission System Operators for Electricity [69]. However, these requirements should account for the operating condition of wind generators because the WTGs operating at low power have a limited ability to respond. The fast fault current injection requirement should consider its impact on DC-link voltage regulation to ensure that the WTG can restore to normal operation after disturbance. The challenges and opportunities from GFM inverter-based resources have been discussed by Western Electricity Coordinating Council (WECC), and Energy Systems Integration Group (ESIG) [70].

2) *Modeling of GFM WTG for large-scale system studies*: The generic wind turbine models have been developed by Western Electricity Coordinating Council (WECC) [71] and International Electrotechnical Commission (IEC) [72] for transient studies of large-scale wind farms. However, these models were developed for the GFL WTG. The generic WECC model has been improved to represent the behavior of GFM inverters [73]. Phasor-approximation model has been developed in [74] for RMS modeling of GFM inverters. Three-phase electromechanical models of GFL and GFM inverters have been developed in [75] for dynamic simulation of the large-scale unbalanced distribution system. Nevertheless, the standards-compliant model is required for electromagnetic transient studies of large-scale wind farms.

3) *Integrated energy storage system*: ESS integrated into WTG would release the grid-side converter from the main wind turbine controllers. Thus, most existing GFM methodologies can be applied for the grid-side converter as the DC-link voltage is controlled by the integrated ESS [76]. In addition, the integrated ESS would play the role of energy buffer, which is an important factor to address the uncertain characteristic of wind power [77], [78]. Practical experience of GFM WTG in [8] has revealed that the turbine's ability to respond to the disturbance may be affected if the wind speed is declining or the WTG operates at low power. The integrated ESS would help the GFM WTG have the ability to respond to the grid disturbance in such conditions.

4) *Testing and Validating GFM WTG*: The successful testing of a 69MW wind park operating in GFM mode demonstrates GFM wind turbines' feasibility [7], [8]. However, there is a lack of explicit criteria for the functionality and performance of GFM WTG. Standardized guidelines on the

testing and validating are needed to assess the GFM controls of WTG, which should be clearly defined in standards or grid codes.

VI. CONCLUSION

This paper provides an overview of grid-forming wind turbine generators and discusses the implementations of different GFM categories. This paper discusses four GFM methodologies: multi-loop GFM (S-MGFM and M-MGFM) and single-loop GFM (S-SGFM and M-SGFM). A comparative study has been conducted to evaluate their performances. It is observed that the M-MGFM and M-SGFM types provide a better performance as the DC-link voltage is controlled by the machine-side converter which is decoupled from the grid's disturbance. The tested result under fault conditions shows that the single-loop GFM types have a higher stability margin than the multi-loop GFM types. This paper reveals that the DC-link voltage has a significant impact on the performance of the GFM WTG. Because the GFM WTGs respond quickly to the disturbance while the electric power from PMSG changes slowly, DC power from the DC link is drawn to compensate for the disturbance, resulting in the rapid drop of DC-link voltage. This issue causes a severe impact on the performance of grid-side converters under fault conditions. However, it is ignored in the design of existing GFM controls. For the design of GFM WTGs, this issue should be taken into consideration. Finally, recommendations and future trends of GFM WTGs have been provided.

REFERENCES

- [1] G. R. Energy, "Haliade-x offshore wind turbine platform," <https://www.ge.com/renewableenergy/wind-energy/offshore-wind/haliade-x-offshore-turbine>, accessed: 2021-08-28.
- [2] Vestas, "Offshore wind turbine platform v164-10.0 mw," <https://www.vestas.com/en/products/offshore-platforms/v164-10-0-mw>, accessed: 2021-08-27.
- [3] ———, "Offshore wind turbine platform v236-15.0 mw," <https://www.vestas.com/en/products/offshore-platforms/v236-15-mw>, accessed: 2021-08-27.
- [4] E. Gaertner, J. Rinker, L. Sethuraman, F. Zahle, B. Anderson, G. E. Barter, N. J. Abbas, F. Meng, P. Bortolotti, W. Skrzypinski *et al.*, "Iea wind tcp task 37: definition of the iea 15-megawatt offshore reference wind turbine," National Renewable Energy Lab.(NREL), Golden, CO (United States), Tech. Rep., 2020.
- [5] R. Rosso, X. Wang, M. Liserre, X. Lu, and S. Engelken, "Grid-forming converters: Control approaches, grid-synchronization, and future trends—a review," *IEEE Open Journal of Industry Applications*, vol. 2, pp. 93–109, 2021.
- [6] C. Yang, L. Huang, H. Xin, and P. Ju, "Placing grid-forming converters to enhance small signal stability of pll-integrated power systems," *IEEE Transactions on Power Systems*, vol. 36, no. 4, pp. 3563–3573, 2021.
- [7] A. Roscoe, T. Knuoppel, R. Da Silva, P. Brogan, I. Gutierrez, D. Elliott, and J.-C. Perez Campion, "Response of a grid forming wind farm to system events, and the impact of external and internal damping," *IET Renewable Power Generation*, vol. 14, no. 19, pp. 3908–3917, 2020.
- [8] A. Roscoe, P. Brogan, D. Elliott, T. Knuoppel, I. Gutierrez, J. Perez Campion, and R. Da Silva, "Practical experience of operating a grid forming wind park and its response to system events," in *Proceeding of the 18th Wind Integration Workshop, Dublin, Ireland*, 2019, pp. 16–18.
- [9] A. AVAZOV, "Application of input shaping method to vibrations damping in a type-iv wind turbine interfaced with a grid-forming converter," 2021.
- [10] Y. Li, X. Yuan, J. Li, H. Xiao, Z. Xu, and Z. Du, "Novel grid-forming control of pmsg-based wind turbine for integrating weak ac grid without sacrificing maximum power point tracking," *IET Generation, Transmission & Distribution*, vol. 15, no. 10, pp. 1613–1625, 2021.
- [11] A. Jain, J. N. Sakamuri, and N. A. Cutululis, "Grid-forming control strategies for black start by offshore wind power plants," *Wind Energy Science*, vol. 5, no. 4, pp. 1297–1313, 2020.
- [12] S. S. H. Yazdi, J. Milimonfared, S. H. Fathi, K. Rouzbeh, and E. Rakhshani, "Analytical modeling and inertia estimation of vsg-controlled type 4 wtgs: Power system frequency response investigation," *International Journal of Electrical Power & Energy Systems*, vol. 107, pp. 446–461, 2019.
- [13] Y. Lin, J. H. Eto, B. B. Johnson, J. D. Flicker, R. H. Lasseter, H. N. Villegas Pico, G.-S. Seo, B. J. Pierre, and A. Ellis, "Research roadmap on grid-forming inverters," National Renewable Energy Lab.(NREL), Golden, CO (United States), Tech. Rep., 2020.
- [14] R. H. Lasseter, Z. Chen, and D. Pattabiraman, "Grid-forming inverters: A critical asset for the power grid," *IEEE Journal of Emerging and Selected Topics in Power Electronics*, vol. 8, no. 2, pp. 925–935, 2020.
- [15] J. Matevosyan, B. Badrzadeh, T. Prevost, E. Quitmann, D. Ramasubramanian, H. Urdal, S. Achilles, J. MacDowell, S. H. Huang, V. Vital, J. O'Sullivan, and R. Quint, "Grid-forming inverters: Are they the key for high renewable penetration?" *IEEE Power and Energy Magazine*, vol. 17, no. 6, pp. 89–98, 2019.
- [16] E. Rokrok, T. Qoria, A. Bruyere, B. Francois, and X. Guillaud, "Classification and dynamic assessment of droop-based grid-forming control schemes: Application in hvdc systems," *Electric Power Systems Research*, vol. 189, p. 106765, 2020.
- [17] V. Yaramasu and B. Wu, "Power electronics for high-power wind energy conversion systems," in *Encyclopedia of Sustainable Technologies*, M. A. Abraham, Ed. Oxford: Elsevier, 2017, pp. 37–49.
- [18] F. Blaabjerg and K. Ma, "Wind energy systems," *Proceedings of the IEEE*, vol. 105, no. 11, pp. 2116–2131, 2017.
- [19] T.-T. Nguyen and H.-M. Kim, "Leader-following diffusion-based reactive power coordination and voltage control of offshore wind farm," *IEEE Access*, vol. 8, pp. 149 555–149 568, 2020.
- [20] T.-T. Nguyen, T. Vu, T. Ortmeyer, G. Stefopoulos, G. Pedrick, and J. MacDowell, "Real-time modeling of offshore wind turbines for transient simulation and studies," in *IECON 2021 – 47th Annual Conference of the IEEE Industrial Electronics Society*, 2021, pp. 1–6.
- [21] S. M. Muyeen, R. Takahashi, T. Murata, and J. Tamura, "A variable speed wind turbine control strategy to meet wind farm grid code requirements," *IEEE Transactions on Power Systems*, vol. 25, no. 1, pp. 331–340, 2010.
- [22] W. Li, G. Joos, and J. Belanger, "Real-time simulation of a wind turbine generator coupled with a battery supercapacitor energy storage system," *IEEE Transactions on Industrial Electronics*, vol. 57, no. 4, pp. 1137–1145, 2010.
- [23] Y. Li, Z. Xu, and K. P. Wong, "Advanced control strategies of pmsg-based wind turbines for system inertia support," *IEEE Transactions on Power Systems*, vol. 32, no. 4, pp. 3027–3037, 2016.
- [24] J. He, K. Wu, L. Huang, H. Xin, C. Lu, and H. Wang, "A coordinated control scheme to realize frequency support of pmsg-based wind turbines in weak grids," in *2018 IEEE Power & Energy Society General Meeting (PESGM)*. IEEE, 2018, pp. 1–5.
- [25] S. Sang, C. Zhang, X. Cai, M. Molinas, J. Zhang, and F. Rao, "Control of a type-iv wind turbine with the capability of robust grid-synchronization and inertial response for weak grid stable operation," *IEEE Access*, vol. 7, pp. 58 553–58 569, 2019.
- [26] Y. Wang, J. Meng, X. Zhang, and L. Xu, "Control of pmsg-based wind turbines for system inertial response and power oscillation damping," *IEEE Transactions on Sustainable Energy*, vol. 6, no. 2, pp. 565–574, 2015.
- [27] K. Günther and C. Sourkounis, "Investigation of virtual synchronous machine control for the grid-side converter of wind turbines with permanently excited synchronous generator," in *IECON 2019-45th Annual Conference of the IEEE Industrial Electronics Society*, vol. 1. IEEE, 2019, pp. 2395–2401.
- [28] J. Xi, H. Geng, G. Yang, and S. Ma, "Inertial response analysis of pmsg-based wecs with vsg control," *The Journal of Engineering*, vol. 2017, no. 13, pp. 897–901, 2017.
- [29] D. Duckwitz, M. Shan, and B. Fischer, "Synchronous inertia control for wind turbines," in *13th Wind Integration Workshop, Conf. Proc., Berlin*, 2014.
- [30] Q.-C. Zhong, Z. Ma, W.-L. Ming, and G. C. Konstantopoulos, "Grid-friendly wind power systems based on the synchronverter technology," *Energy Conversion and Management*, vol. 89, pp. 719–726, 2015.
- [31] Y. Ma, W. Cao, L. Yang, F. Wang, and L. M. Tolbert, "Virtual synchronous generator control of full converter wind turbines with short-term energy storage," *IEEE Transactions on Industrial Electronics*, vol. 64, no. 11, pp. 8821–8831, 2017.
- [32] Y. Ma, L. Yang, F. Wang, and L. M. Tolbert, "Voltage closed-loop virtual synchronous generator control of full converter wind turbine for grid-connected and stand-alone operation," in *2016 IEEE Applied Power Electronics Conference and Exposition (APEC)*. IEEE, 2016, pp. 1261–1266.

[33] Y. Liu, X. Zhou, and S. Ouyang, "Capacitor voltage synchronising control-based vsg scheme for inertial and primary frequency responses of type-4 wtgs," *IET Generation, Transmission & Distribution*, vol. 12, no. 14, pp. 3461–3469, 2018.

[34] X. He, S. Pan, and H. Geng, "Transient stability of hybrid power systems dominated by different types of grid-forming devices," *IEEE Transactions on Energy Conversion*, pp. 1–1, 2021.

[35] D. B. Rathnayake, M. Akrami, C. Phurailatpam, S. P. Me, S. Hadavi, G. Jayasinghe, S. Zabihi, and B. Bahrami, "Grid forming inverter modeling, control, and applications," *IEEE Access*, vol. 9, pp. 114 781–114 807, 2021.

[36] D. Pan, X. Wang, F. Liu, and R. Shi, "Transient stability of voltage-source converters with grid-forming control: A design-oriented study," *IEEE Journal of Emerging and Selected Topics in Power Electronics*, vol. 8, no. 2, pp. 1019–1033, 2020.

[37] I. Sadeghkhani, M. E. Hamedani Golshan, J. M. Guerrero, and A. Mehrizi-Sani, "A current limiting strategy to improve fault ride-through of inverter interfaced autonomous microgrids," *IEEE Transactions on Smart Grid*, vol. 8, no. 5, pp. 2138–2148, 2017.

[38] W. Du and R. H. Lasseter, "Overload mitigation control of droop-controlled grid-forming sources in a microgrid," in *2017 IEEE Power Energy Society General Meeting*, 2017, pp. 1–5.

[39] W. Du, Z. Chen, K. P. Schneider, R. H. Lasseter, S. Pushpak Nandanoori, F. K. Tuffner, and S. Kundu, "A comparative study of two widely used grid-forming droop controls on microgrid small-signal stability," *IEEE Journal of Emerging and Selected Topics in Power Electronics*, vol. 8, no. 2, pp. 963–975, 2020.

[40] E. Rokrok, T. Qoria, A. Bruyere, B. Francois, and X. Guillaud, "Transient stability assessment and enhancement of grid-forming converters embedding current reference saturation as current limiting strategy," *IEEE Transactions on Power Systems*, 2021.

[41] K. V. Kkuni and G. Yang, "Effects of current limit for grid forming converters on transient stability: analysis and solution," 2021.

[42] T. Qoria, F. Gruson, F. Colas, X. Kestelyn, and X. Guillaud, "Current limiting algorithms and transient stability analysis of grid-forming vscs," *Electric Power Systems Research*, vol. 189, p. 106726, 2020.

[43] R. Rosso, S. Engelken, and M. Liserre, "On the implementation of an frt strategy for grid-forming converters under symmetrical and asymmetrical grid faults," *IEEE Transactions on Industry Applications*, vol. 57, no. 5, pp. 4385–4397, 2021.

[44] M. G. Taul, X. Wang, P. Davari, and F. Blaabjerg, "Current limiting control with enhanced dynamics of grid-forming converters during fault conditions," *IEEE Journal of Emerging and Selected Topics in Power Electronics*, vol. 8, no. 2, pp. 1062–1073, 2019.

[45] X. Zhao and D. Flynn, "Freezing grid-forming converter virtual angular speed to enhance transient stability under current reference limiting," in *2020 IEEE 21st Workshop on Control and Modeling for Power Electronics (COMPEL)*. IEEE, 2020, pp. 1–7.

[46] M. Awal and I. Husain, "Transient stability assessment for current constrained and unconstrained fault ride-through in virtual oscillator controlled converters," *IEEE Journal of Emerging and Selected Topics in Power Electronics*, 2021.

[47] C. Liu, X. Cai, R. Li, and R. Yang, "Optimal short-circuit current control of the grid-forming converter during grid fault condition," *IET Renewable Power Generation*, 2021.

[48] T. Qoria, F. Gruson, F. Colas, G. Denis, T. Prevost, and X. Guillaud, "Critical clearing time determination and enhancement of grid-forming converters embedding virtual impedance as current limitation algorithm," *IEEE Journal of Emerging and Selected Topics in Power Electronics*, vol. 8, no. 2, pp. 1050–1061, 2019.

[49] Y. Li, L. Fan, and Z. Miao, "Replicating real-world wind farm sss events," *IEEE Transactions on Power Delivery*, vol. 35, no. 1, pp. 339–348, 2020.

[50] X. Xie, W. Liu, J. Shair, C. Dai, and X. Liu, "Subsynchronous control interaction: Real-world events and practical impedance reshaping controls."

[51] A. K. Moharana, "Subsynchronous resonance in wind farms," 2012.

[52] G. Li, Y. Chen, A. Luo, Z. He, H. Wang, Z. Zhu, W. Wu, and L. Zhou, "Analysis and mitigation of subsynchronous resonance in series-compensated grid-connected system controlled by a virtual synchronous generator," *IEEE Transactions on Power Electronics*, vol. 35, no. 10, pp. 11 096–11 107, 2020.

[53] G. P. Prajapat, N. Senroy, and I. N. Kar, "Wind turbine structural modeling consideration for dynamic studies of dfig based system," *IEEE Transactions on Sustainable Energy*, vol. 8, no. 4, pp. 1463–1472, 2017.

[54] M. Edrah, X. Zhao, W. Hung, P. Qi, B. Marshall, A. Karcanias, and S. Baloch, "Effects of pod control on a dfig wind turbine structural system," *IEEE Transactions on Energy Conversion*, vol. 35, no. 2, pp. 765–774, 2020.

[55] A. D. Hansen, N. A. Cutululis, H. Markou, P. Sørensen, and F. Iov, "Grid fault and design-basis for wind turbines. final report," 2010.

[56] A. D. Hansen, N. A. Cutululis, H. Markou, and P. E. Sørensen, "Impact of fault ride-through requirements on fixed-speed wind turbine structural loads," *Wind Energy*, vol. 14, no. 1, pp. 1–11, 2011.

[57] M. Edrah, X. Zhao, W. Hung, P. Qi, B. Marshall, S. Baloch, and A. Karcanias, "Electromechanical interactions of full scale converter wind turbine with power oscillation damping and inertia control," *International Journal of Electrical Power & Energy Systems*, vol. 135, p. 107522, 2022.

[58] E. Mohammadi, R. Fadaeinedjad, and G. Moschopoulos, "Implementation of internal model based control and individual pitch control to reduce fatigue loads and tower vibrations in wind turbines," *Journal of sound and vibration*, vol. 421, pp. 132–152, 2018.

[59] T. Lund, B. Yin, G. K. Andersen, M. Gupta, and G. Interconnection, "Challenges and solutions for integration of wind power in weak grid areas with high inverter penetration."

[60] S. K. Mutha, A. Shrestha, V. Cecchi, and M. Manjrekar, "Analysis of negative-sequence directional element for type-iv wind power plants under various control methodologies," in *2020 52nd North American Power Symposium (NAPS)*, 2021, pp. 1–6.

[61] V. VDE-AR-N, "4120," *Technical Requirements for the Connection and Operation of Customer Installations to the High Voltage Network (TAB High Voltage)*.

[62] B. Mahamed, M. Eskandari, J. E. Fletcher, and J. Zhu, "Sequence-based control strategy with current limiting for the fault ride-through of inverter-interfaced distributed generators," *IEEE Transactions on Sustainable Energy*, vol. 11, no. 1, pp. 165–174, 2020.

[63] M. A. Awal, M. R. K. Rachi, H. Yu, I. Husain, and S. Lukic, "Double synchronous unified virtual oscillator control for asymmetrical fault ride-through in grid-forming voltage source converters," Jun 2021.

[64] N. S. Gurule, J. Hernandez-Alvidrez, R. Darbali-Zamora, M. J. Reno, and J. D. Flicker, "Experimental evaluation of grid-forming inverters under unbalanced and fault conditions," in *IECON 2020 The 46th Annual Conference of the IEEE Industrial Electronics Society*. IEEE, 2020, pp. 4057–4062.

[65] "Ieee standard for interconnection and interoperability of distributed energy resources with associated electric power systems interfaces," *IEEE Std 1547-2018 (Revision of IEEE Std 1547-2003)*, pp. 1–138, 2018.

[66] NERC, "Standard prc-024-2 — generator frequency and voltage protective relay settings," 2016.

[67] N. R. Guideline, "Bps-connected inverter-based resource performance," *North American Electric Reliability Corporation (NERC): Atlanta, GA, USA*, 2018.

[68] N. G. ESO, "Gc0137: Minimum specification required for provision of gb grid forming (gbgf) capability (formerly virtual synchronous machine/vsm capability)," National Grid ESO, Gallows Hill, Warwick (United Kingdom). Tech. Rep., 2020.

[69] E. N. of Transmission System Operators for Electricity, "High penetration of power electronic interfaced power sources and the potential contribution of grid forming converters," Tech. Rep., 2020.

[70] ESIG, "Wecc/esig grid-forming inverter-based resources workshop," <https://www.esig.energy/event/wecc-esig-grid-forming-inverter-based-resources-workshop/>, accessed: 2021-11-16.

[71] W. REMTF, "Wecc second generation of wind turbines models guidelines," *WECC, USA*, 2014.

[72] A. Lorenzo-Bonache, A. Honrubia-Escribano, F. Jiménez-Buendía, and E. Gómez-Lázaro, "Field validation of generic type 4 wind turbine models based on iec and wecc guidelines," *IEEE Transactions on Energy Conversion*, vol. 34, no. 2, pp. 933–941, 2019.

[73] D. Ramasubramanian, P. Pourbeik, E. Farantatos, and A. Gaikwad, "Simulation of 100IEEE Electrification Magazine," vol. 9, no. 2, pp. 62–71, 2021.

[74] G. S. Misyris, S. Chatzivasileiadis, and T. Weckesser, "Grid-forming converters: Sufficient conditions for rms modeling," *Electric Power Systems Research*, vol. 197, p. 107324, 2021.

[75] W. Du, F. K. Tuffner, K. P. Schneider, R. H. Lasseter, J. Xie, Z. Chen, and B. Bhattachari, "Modeling of grid-forming and grid-following inverters for dynamic simulation of large-scale distribution systems," *IEEE Transactions on Power Delivery*, vol. 36, no. 4, pp. 2035–2045, 2020.

[76] G. Xu, L. Xu, D. J. Morrow, and D. Chen, "Coordinated dc voltage control of wind turbine with embedded energy storage system," *IEEE Transactions on Energy Conversion*, vol. 27, no. 4, pp. 1036–1045, 2012.

[77] T. H. Nguyen and D.-C. Lee, "Advanced fault ride-through technique for pmag wind turbine systems using line-side converter as statcom," *IEEE Transactions on Industrial Electronics*, vol. 60, no. 7, pp. 2842–2850, 2013.

[78] C. Kim and W. Kim, "Low-voltage ride-through coordinated control for pmag wind turbines using de-loaded operation," *IEEE Access*, vol. 9, pp. 66 599–66 606, 2021.